

Straintronics in Phosphorene: Tensile vs Shear Strains and Their Combinations for Manipulating the Band Gap

Anastasiia G. Solomenko¹, Ihor Y. Sahalianov², Taras M. Radchenko^{1,*},
and Valentyn A. Tatarenko¹

¹Department of Metallic State Theory, G. V. Kurdyumov Institute for Metal Physics of the N.A.S. of Ukraine, UA-03142 Kyiv, Ukraine

²Laboratory of Organic Electronics, Department of Science and Technology, Linköping University, SE-60174 Norrköping, Sweden

*tarad@imp.kiev.ua

Abstract

We study the effects of the uniaxial tensile strain and shear deformation as well as their combinations on the electronic properties of single-layer black phosphorene. The evolutions of the strain-dependent band gap are obtained using the numerical calculations within the tight-binding (TB) model as well as the first-principles (DFT) simulations and compared with previous findings. The TB-model-based findings show that the band gap of the strain-free phosphorene agrees with the experimental value and linearly depends on both stretching and shearing: increases (decreases) as the stretching increases (decreases), whereas gradually decreases with increasing the shear. A linear dependence is less or more similar as compared to that obtained from the *ab initio* simulations for shear strain, however disagrees with a non-monotonic behaviour from the DFT-based calculations for tensile strain. Possible reasons for the discrepancy are discussed. In case of a combined deformation, when both strain types (tensile/compression + shear) are loaded simultaneously, their mutual influence extends the realizable band gap range: from zero up to the values respective to the wide-band-gap semiconductors. At a switched-on combined strain, the semiconductor–semimetal phase transition in the phosphorene is reachable at a weaker (strictly non-destructive) strain, which contributes to progress in fundamental and breakthroughs.

Introduction: background of the problem and motivation of the study

The post-graphene era of two-dimensional or quasi-two-dimensional (2D) materials¹ got an additional impact for further development when in 2014 two different groups^{2,3} independently exfoliated the single-layer black phosphorus — called “phosphorene” (further in the text mentioning phosphorene, we will mean black one) — from the bulk black phosphorus, which in turn has been first synthesized more than century ago^{4,5}. Phosphorus is one of the abundant chemical elements in the Earth’s crust (up to $\approx 0.1\%$)^{6,7} and black P (α -form) is the most thermodynamically stable at ambient conditions among other phosphorus allotropes (white, red, violet, and A7 phase)^{8,9}. Since 2014, extensive studies are carried out to promote the investigations of phosphorene: hundreds and even thousands of papers dealing with this material have been already published all over the world (*e.g.*, each of the Web of Science and Scopus scientometric databases numbers almost two thousands of articles containing the word “phosphorene” straight in the title).

As distinct from graphene, which is flatness (atomically flat), the crystal structure of phosphorene represents a corrugated atomic monolayer (see Fig. 1a–d), where chains of covalently bonded P atoms reside in two different planes. Among the family of currently known 2D materials, the monolayer black phosphorus attracts attention as a promising candidate not only for (opto)electronics, but for all material science as an interesting object for detailed study due to its peculiar features. Phosphorene has a natural direct band gap in the centre (Γ -point) of the Brillouin zone (Fig. 1e); however, its calculated value strongly differs in the literature from 0.76 to 2.31 eV (see collected data in tables^{10,11} and Çakır *et al.*¹²) depending on the computational methods and approximations. At the same time, the experimentally measured gap value turned out also quite different: from 1.45 eV² to 2.05 eV¹³ and 2.2 eV¹⁴ (whereas for bulk black phosphorus, the gap is 0.31–0.36 eV^{15–18}). Some authors claimed even higher band gap values: up to 2.2 eV. Phosphorene exhibits a high on/off current ratio (up to $\sim 10^5$)¹⁹ and (ambipolar)²⁰ carrier mobility (from 600 $\text{cm}^2\text{V}^{-1}\text{s}^{-1}$ at room temperature²¹ up to $\sim 10^3$ $\text{cm}^2\text{V}^{-1}\text{s}^{-1}$ at 120 K and even higher at lower temperatures²², *i.e.*, comparable with graphene). It is most remarkable and that is why worthy of attention features are high anisotropy (in mechanical, electronic, optical, thermal, and transport properties)^{19,23–25}, as a response to the anisotropy of the puckered (called also as buckled or wrinkled) lattice, and superior mechanical properties^{26,27}.

Due to the extraordinary mechanical flexibility, phosphorene can sustain the elastic deformations up to (its failure limits) $\approx 27\text{--}30\%$ at single-axial strain²⁶ (which corresponds to the stress

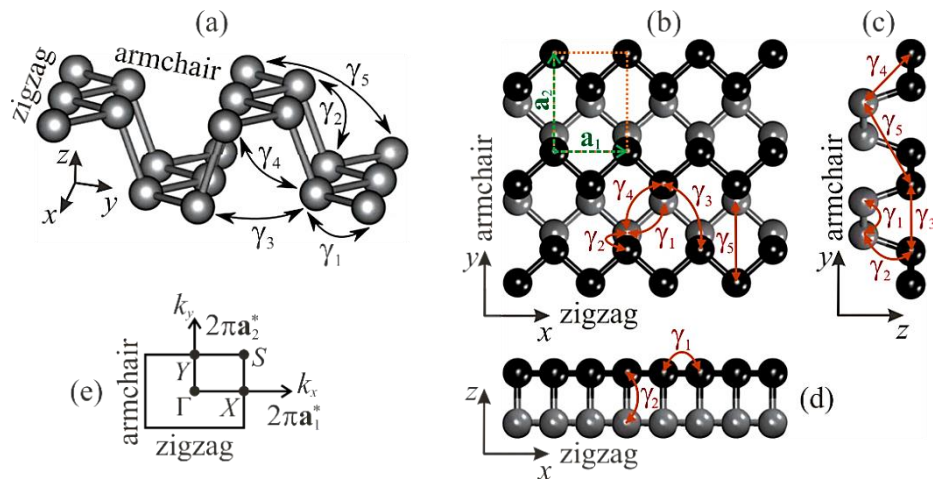


Figure 1. Crystal lattice of black phosphorene: perspective (a), top (b), and side (c, d) views. Black and grey balls in (b–d) depict the upper and lower sublayers of P atoms, respectively. Dashed rectangle in (b) outlines the basic unit cell (without taking into account the vacuum) with the basis translation vectors \mathbf{a}_1 and \mathbf{a}_2 . The five non-equivalent hopping parameters in (a–d) are denoted by $\gamma_1, \gamma_2, \dots, \gamma_5$. Solid rectangle (e) exhibits the first Brillouin zone projected on xy -plane, where Γ, X, Y, S are the non-equivalent high-symmetry points in the reciprocal \mathbf{k} -space with the basis translation vectors \mathbf{a}_1^* and \mathbf{a}_2^* .

up to ≈ 10 N/m)²⁷ depending on the stretching direction, and up to ≈ 10 –13% at shear strains^{28,29}. However, other authors claim about non-destructive $\approx 48\%$ ($\approx 11\%$) uniaxial deformation along armchair (zigzag) direction²⁴ and 30–35% shear strains³⁰. If the isotropic strain reaches 29%, the puckered phosphorene structure transforms into a plane hexagonal flat lattice³¹. On one hand, such an enormous mechanical flexibility indicates the potential application at extreme conditions. On another hand, it offers an opportunity to consider this material (following graphene)^{32,33} as an eminently suitable object of the study within the still relatively new research field in the condensed matter physics known as “straintronics”^{34–37}, in which the strain-induced physical effects in solids act as a tool for tuning (even amendment if any) the electronic properties. In the context of unique mechanical properties of phosphorene, another intriguing feature is its ability to be an auxetic, which is originated from its puckered structure. The existence of a negative Poisson’s ratio ν in the out-of-plane direction under the uniaxial stretching in the direction parallel to the pucker, *i.e.*, along zigzag (x as denoted in Fig. 1) direction, was revealed in several works^{31,38–40}, where a great difference of ν in different directions reflects the strong structural anisotropy. It is considered that phosphorene is a first known 2D auxetic material.

Similarly to its forefather, — graphene,^{41,42} — the sensitivity of phosphorene’s electronic structure to the external perturbations has noticed attention of researchers and as a result caused quite a number of mainly theoretical (analytical or/and computational) studies dealing with the response of the band gap behaviour on the mechanical field influence. Such a field is reflected in the axial (uni-, bi-, and even tri-axial) and isotropic tensile (or compression as a negative extension) strains. Rodin *et al.*⁴³ and Hien *et al.*⁴⁴ predicted the gap closing upon moderate compression along the transverse (out-of-plane) z direction in phosphorene (see Fig. 1a–d). However, according to Li *et al.*⁴⁵, for the band gap closing, the biaxial compressive strain of 9% is required, while Hu *et al.*³¹ assert about isotropic 7% compression or 22% stretching for the gap closing. Appearance of the semi-metallic and insulating (more than 3 eV gap) phases in phosphorene at the uniaxial + biaxial deformations in the range of $\pm 20\%$ along the armchair (Γ – Y) and zigzag (Γ – X) directions (see Fig. 1e) predicted by Yarmohammadi with co-authors⁴⁶, where they obtained the band gap for unstrained phosphorene as 1.52 eV. In contrast to them, some other authors^{31,38,43,47} claimed different band gap values (at the Γ -point) of unstrained phosphorene: from 0.7–0.95 eV^{31,39,43,47} up to 2.31 eV¹² depending on the approximations and computation schemes have been used. Phuc *et al.*⁴⁷ also observed a semiconductor–semimetal transition at the compression of 13% or 10% along the armchair and zigzag direction, respectively; moreover, even transition to the metallic state at the larger compressions. This disagrees with Elahi *et al.*³⁹, who reported about other strains of such a transition. In addition to the magnitude of the band gap, its type (direct–indirect) also undergoes the deformation-induced changing from direct to indirect and vice versa as many authors argue^{27,31,39,47,48}. They report a whole number of cases when they observed such a transition for different strain types and values. Sometimes these values and types of such a critical strain even contradict each other. Interestingly, that appropriate interplanar (*e.g.*, uniaxial or biaxial) strain can even rotate the preferred electrical conducting direction in phosphorene⁴⁹.

There is still a lack of studies of phosphorene under elastic shear strain — another important and commonly occurred external stress for graphene^{50,51} and other members of the 2D materials’ family⁵². As well as the tensile deformation, such a strain type can be realized in different forms, *e.g.*, global shear deformation, process-induced or post-processing shearing²⁸. At present, we found only three works (two computational^{28,30} and one analytical⁵³) reporting on the influence of shear strain on electronic structure and properties of phosphorene. The case of simultaneous effect of both (tensile and shear) strain types is found in one work⁵³ only, where authors reported that the most effective, *i.e.*, large, band gap manipulation does not require strongly armchair or zigzag direction. They⁵³ claim that the optimal strain direction depends rather on its type, and predict the combination of uniaxial armchair strain and shear deformation as the most effective approach to enlarging the bandgap. The statement about insignificance of the strain direction on its effectiveness⁵³ contradicts to the statement of Wang *et al.*⁵⁴ that the gap enlarges with the changing the direction of stress from zigzag to armchair.

Summarizing the results, we analysed in the above-mentioned briefly reviewed articles, one can emphasize on the following moments. (i) The lion’s share of them reports on the results obtained from computations. In such computational studies, authors used commonly the VASP^{2,10,27,28,45, 55} or

Quantum ESPRESSO^{30,43,47,49} and rarely other simulation packages like SIESTA^{2,12,56}, ABINIT⁴⁸ or VNL-ATK⁵⁷ for performing the density-functional theory first-principles calculations. Such calculations are suitable, accurate, and fruitful, however computationally expensive since require high computational capabilities (even implemented in the author's program code^{58–60}). *Ab initio* calculations are not feasible for large or moderate scale systems. Therefore, the phosphorene computational-domain sizes in such calculations are restricted to one or several unite cells, periodic supercells or lattice fragments with a relatively small (up to several dozens) quantity of the lattice sites (atoms). (ii) Although all authors report on the phosphorene as a superconductor with moderate energy gap, the reported gap values differ from each other more than 150% (even for the unstrained sample), which seems quite a lot. The calculated values depend on the applied computational methods and model approximations. All authors claim about deformational tunability of the band gap, however there is a lack of uniqueness on the strain type and values resulting in increasing (decreasing) the gap up (down) to the insulator (semimetal) state. (iii) There is a deficiency in the study of the shear strain effects on the phosphorene electronic structure, particularly on its band gap behaviour, especially as because this strain type can be dominated in the 2D-sheets-based flexible electronics⁶¹.

Motivated by the restrictions, discrepancies, and scarcity indicated above in pts. (i)–(iii), respectively, in this work we use the analytical model of the tight-binding approximation with distant-dependent hopping integrals and Green's function method for implementation into the efficient numerical methodology of calculation of density of electronic states followed by the extraction of the band gap in phosphorene subjected to the uniaxial intraplanar tensile and shear strains as well as their combinations. At that, our computational domain contains millions of atoms, *i.e.*, close to realistic samples. In addition, we also use the first-principles calculations based on a density functional theory implemented in the Quantum Espresso package to compare our results obtained within both methods as well as with findings of other authors.

Theoretical and numerical approaches

Tight-binding Hamiltonian

Within the framework of the effective tight-binding (TB) model, the Hamiltonian in a real-space representation is defined on a phosphorene lattice as^{44,46,62–65}

$$\hat{H} = \sum_{i \neq j} \gamma_{ij} c_i^\dagger c_j + \text{H.c.} = \gamma_1 \sum_{i \neq j} c_i^\dagger c_j + \gamma_2 \sum_{i \neq j} c_i^\dagger c_j + \gamma_3 \sum_{i \neq j} c_i^\dagger c_j + \gamma_4 \sum_{i \neq j} c_i^\dagger c_j + \gamma_5 \sum_{i \neq j} c_i^\dagger c_j + \dots, \quad (1)$$

where indices i and j run over all phosphorene-lattice-sites, c_i^\dagger (c_j) is the fermionic creation (annihilation) operator of electrons at i (j) site, and $\gamma_{ij} = \gamma_{ji}$ are the hopping parameters between the sites i (j) and j (i), and H.c. reflects the Hermitian conjugate of creation and annihilation operators. In our model, we take into account five nearest neighbour hopping integrals $\gamma_1, \gamma_2, \gamma_3, \gamma_4, \gamma_5$ denoted in Fig. 1a–d; thus, the summation in Eq. (1) is carried out up to the fifth neighbours. Note that the Hamiltonian in Eq. (1) does not contain any on-site term, in contrast to two papers by Katsnelson with co-authors^{66,67}, since here, we consider the defect-free lattice, so electrons have equivalent energies over all sites.

The values of the tight-binding parameters for the unstrained phosphorene lattice were adopted from Rudenko *et al.*⁶⁶: $\gamma_1^0 = -1.22$ eV ($l_1^0 = 0.222$ nm), $\gamma_2^0 = 3.665$ eV ($l_2^0 = 0.224$ nm), $\gamma_3^0 = -0.205$ eV ($l_3^0 = 0.334$ nm), $\gamma_4^0 = -0.105$ eV ($l_4^0 = 0.347$ nm), $\gamma_5^0 = -0.055$ eV ($l_5^0 = 0.423$ nm), where superscript indicates that the system is unstrained (*i.e.*, relaxed or optimized), and values in the brackets—corresponding distances between the lattice sites (see Fig. 1a–d). Authors⁶⁶ used so-called *GW* approximation to obtain the parametrized *GW* Hamiltonian matrix and then extracted hopping energies from this matrix represented in the Wannier-functions' basis $\langle w_i | \hat{H} | w_j \rangle$. Latter these values were also adapted in quite a few other studies^{44,46,64,65,68}. Midtvedt *et al.*⁶³ used a valence-force field model⁶⁹ to obtain an alternative set of the hopping parameters applicable for small and moderate strains <5%.

Strain-caused hopping replacement

We treat of two types of the homogeneous elastic intraplanar deformations: single-axial (Fig. 2a, b)

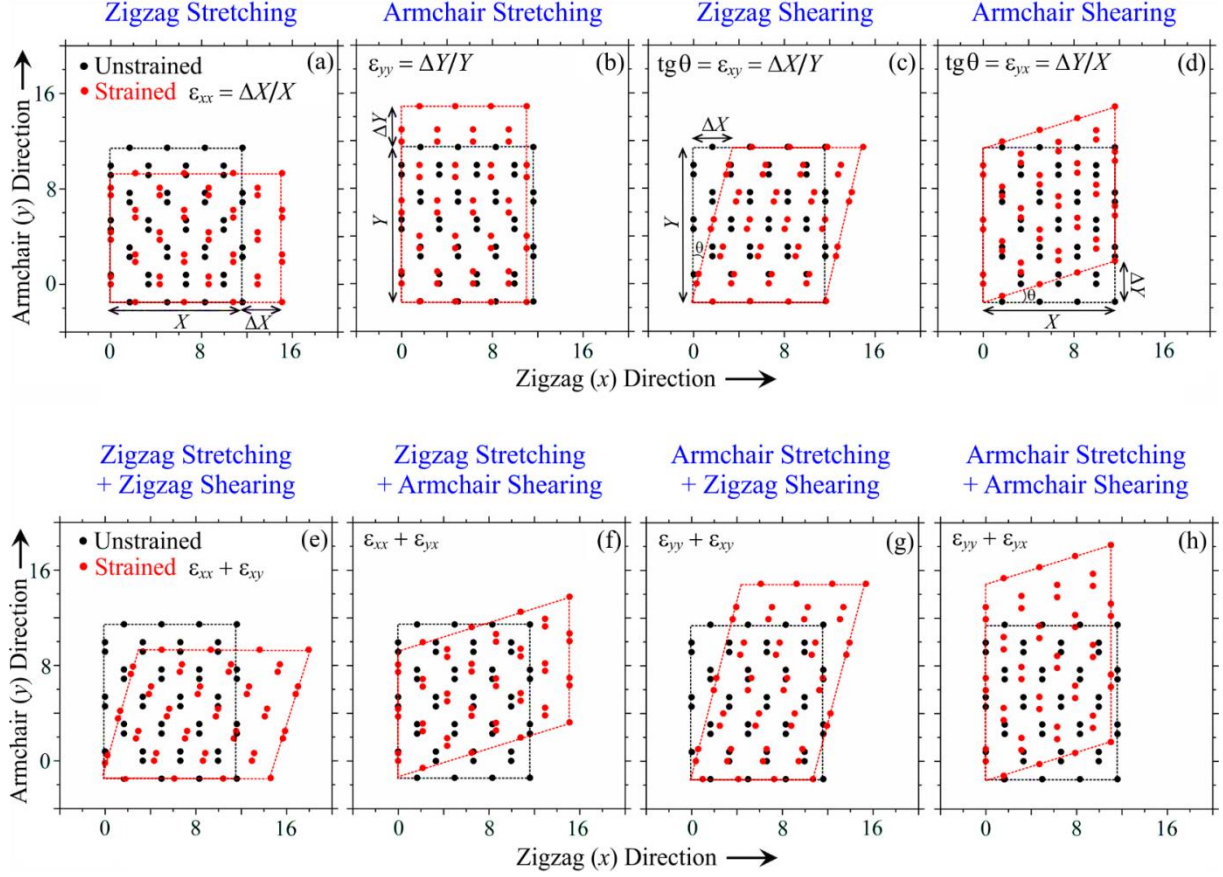


Figure 2. (Colour online) Schematic top views of unstrained and strained black phosphorene lattice as a result of the uniaxial tensile (a, b) or shear (c, d) deformations and their combinations (e–h).

and shear (Fig. 2c, d) strains. For both types, two orthogonally related directions of the applied strain are examined: along the zigzag (Fig. 2a, c) and armchair (Fig. 2b, d) edge. Since in a realistic case, the deformed lattice may be a result of a combination of several strain types, the combined deformation types, — stretching + shearing along one of or both directions (Fig. 2e–h), — are also included.

The uniaxial or/and shear strains induces a lattice deformation for both mutually transverse directions (as well as for any other one), *i.e.*, changes in the interatomic distances (bond lengths l) and bond angles. These values, bond lengths and bond angles, can be changed slightly or strongly depending on the strain type, magnitude and direction; nevertheless, they take the consequences of the change in the hopping integrals between the lattice sites. In a general case, the hoppings can differ among different neighbouring sites. Since we consider a uniform elastic strain, different hopping integrals from a given site to its neighbours should be the same for every such a site. Thus, the model Hamiltonian in Eq. (1) includes five distinct hoppings. As for to the strain-affected graphene^{34,35,41}, we follow the strain-displacement relations⁶³ for a homogeneous elastic strain in phosphorene that can be obtained from a valence-force model⁷⁰ and assume an exponential dependence of the hopping parameters on the interatomic P–P distances l :⁶³

$$\gamma_{ij}(l) = \gamma_{ij}^0 \exp\left(-\beta\left(\frac{|\mathbf{R}'_{ij}|}{|\mathbf{R}_{ij}|} - 1\right)\right), \quad (2)$$

where γ_{ij}^0 is a hopping of unstrained lattice, \mathbf{R}_{ij} (\mathbf{R}'_{ij}) is an original (modified) vector connecting atoms at i - and j -site, $\beta \approx 1.2$ quantifies the decay rate⁷¹, and a transverse response to the applied uniaxial strain (Poisson's effect) is also included. (An alternative way^{44,46,53,64,68,72} to include the strain effect on the hopping parameters in a linear deformation regime is based on the Harrison's rule⁷³ defining the inversely quadratic dependence of the hopping energies on the bond length: $\gamma(l) \propto 1/l^2$.)

Table 1 collects data from several works^{26,27,38,39}, where authors reported on the calculated Poisson's ratios. In contrast to graphene, for which the Poisson's ratio ν is isotropic, in case of

Table 1. In-plane $v_x(y)$, $v_y(x)$ and out-of-plane $v_z(y)$, $v_z(x)$ Poisson's ratios as the responses on the uniaxial stretches oriented along armchair (y) and zigzag (x) directions, respectively, in phosphorene.

	Uniaxial strain direction		Reference
	Armchair (y)	Zigzag (x)	
In-plane v : $v_x(y)$ and $v_y(x)$	0.17	0.62	Wei <i>et al.</i> ²⁶
	0.20	0.70	Peng <i>et al.</i> ²⁷
	0.40	0.93	Jiang <i>et al.</i> ³⁸
	0.24	0.81	Elahi <i>et al.</i> ³⁹
Out-of-plane v : $v_z(y)$ and $v_z(x)$	0.82*	0.50*	Wei <i>et al.</i> ²⁶
	0.046	-0.027	Jiang <i>et al.</i> ³⁸
	0.210	-0.090	Elahi <i>et al.</i> ³⁹

* The out-of-plane Poisson's ratios referred to Wei *et al.*²⁶ are calculated from the ratio of distances between the puckered upper and lower sublayers of the relaxed (*i.e.*, unstrained) phosphorene and uniaxially strained by 30%.

phosphorene v is different for two in-plane (in-layer) stretching directions (along zigzag, x , and armchair, y): $v_y \neq v_x$. Moreover, the out-of-plane (out-of-layer) Poisson's ratio $v_z \neq v_y \neq v_x$ appears and depends on the in-layer uniaxial tensile direction as well. Despite an insignificant inconsistency, the values in Table 1 adequately exhibit an anisotropy in a mechanical response of phosphorene, and a negative out-of-layer Poisson's ratio is revealed^{38,39} along the armchair (y) direction in response to perpendicular (zigzag, x) uniaxial stretch (at least in the strain range of $-5\% \leq \epsilon_{xx} \leq 5\%$)³⁸. In our calculations, we use the in-plane v averaged over those presented in Table 1 for every strain orientation, and the out-of-plane v averaged over data of Jiang *et al.*³⁸ and Elahi *et al.*³⁹ for small or moderate strains ($\leq \pm 5\%$) and adopted from Wei *et al.*²⁶ for larger deformations (up to the predicted failure limit).

TB-model-based computational details

The density of states (DOS) ρ for each energy level E per unit area S and spin relates is defined as

$$\rho(E) = \text{Tr}(\delta(E - \hat{H})/S), \quad (3)$$

where \hat{H} is the Hamiltonian matrix given in Eq. (1). To calculate the DOS of the system, we implement an efficient numerical methodology or algorithm to be more precise, which has been developed earlier for graphene^{41,74}.

The total DOS $\rho(E)$ can be represented as a sum of local density of states (LDOS): $\rho(E) = \sum_i^N \rho_i(E)$ with summation over all phosphorene lattice sites N . The LDOS relates to the imaginary part of the diagonal elements of Green's function^{44,75,76} as $\rho_i(E) = -\pi^{-1} \text{Im} G_{ii}(E + i\zeta)$, where small ζ coefficient smooths peaks in the DOS separated by the energy ranges $\Delta E \propto 1/N$. To calculate the diagonal elements G_{ii} , we have to perform the tridiagonalization procedure for the Hamiltonian (1), which requires the most computational time and depends on the number of sites N . To calculate the first diagonal element of the Green's function G_{11} , we use the continued fraction technique. In principle, if we calculated LDOS at the first site, $\rho_1(E)$, we can repeat such calculations for all other (remaining) $N - 1$ sites in order to obtain the total DOS; however, this procedure requires the computational time quadratically dependent on the size of the system ($\propto N^2$) at issue. Thus, for the realistically large systems with millions of sites (atoms), another method in which the total computational efforts remain to be of the order of N is more reasonable and efficient. Such a method consists in an idea that a sufficiently large subsystem of the total system possesses the same DOS as an original (total) system. We choose a subsystem of ΔN sites at a phosphorene lattice and construct a wave function (packet) $|\psi_{\text{md}}\rangle \equiv \Delta N^{-1/2} \sum_i \exp(2\pi i \alpha_i) |i\rangle$ with the random state over all ΔN sites, random phase $\alpha_i \in [0, 1]$, $|i\rangle \equiv c_i^\dagger |0\rangle$ and summation over all sites of the chosen subsystem ΔN . After that, we transform the origin Hamiltonian (1) through redefining it in another (new) basis and set the wave function $|\psi_{\text{md}}\rangle$ as the first vector in the new basis. Within the tridiagonal representation of the

Hamiltonian and calculating the $\rho_1(E) = -\pi^{-1} \text{Im}G_{11}(E + i\zeta)$ via the continued fraction technique, we obtain the value $\rho_1(E)$ corresponding to the total DOS per one atom (site) of the lattice at hand. Now, there is no any necessity to calculate the remaining $N - 1$ matrix elements G_{ii} , thereby we avoid the quadratic dependence of the computational efforts on the system size and keep the scaling linear ($\propto N$).

The size of the phosphorene lattice, which acts in our calculations as a computational domain, includes 1300×1000 atomic sites along the zigzag (x) and armchair (y) directions, respectively, which corresponds to $\approx 450 \times 450 \text{ nm}^2$, *i.e.*, comparable with realistic phosphorene samples treated in experiments. As mentioned above, to study the strain effect, we subject such a lattice to the uniaxial tensile (Fig. 2a, b) or shear (Fig. 2c, d) deformations as well as their combinations (Fig. 2e–h) when both types of strain are applied. Each of them can be oriented along the zigzag (Fig. 2a, c) or armchair (Fig. 2b, d) directions when they are loaded separately (Fig. 2a–d) or simultaneously (Fig. 2e–h). Tension along any other direction can be represented as a combination of zigzag + armchair stretches.

***Ab initio* computational details**

To evaluate the phosphorene's band structure, — a fundamental information on the electronic properties describing the relationship between the energy and electron wave vectors, — we performed the first principles numerical calculations using the open source computer codes within the Quantum Espresso (QE) electronic-structure simulation package⁷⁷. This package includes the density-functional theory (DFT)⁷⁸, plane wave's basis sets and pseudopotentials to represent the electron-ion interactions. The computation package includes⁷⁷ the calculation of the Kohn–Sham orbitals and energies, complete structural optimizations of the microscopic (atomic coordinates) and macroscopic (unit cell) degrees of freedom, using Hellmann–Feynman forces and stresses. The projector augmented wave (PAW) technique⁷⁹ for generalization of the pseudopotentials, self-consistent total energy calculations and geometry optimization is implemented in the package. The standard generalized gradient approximations (GGA)^{80–82} formalism for the Perdew–Burke–Ernzerhof (PBE)^{83,84} exchange-correlation functional is adopted. The geometry optimization procedure before proceeding to the calculations was required to reach the atomic structure relaxation state. Calculated lattice parameters after the geometry optimization of unstrained lattice were $|\mathbf{a}_1| = 3.344 \text{ \AA}$ and $|\mathbf{a}_2| = 4.588 \text{ \AA}$ (see Fig. 1b) that is in agreement with previous theoretical predictions^{10,11,39,47,48} and the values obtained from experiment⁸⁵. In order to prevent (or at least minimize) interaction between the layers due to the periodic boundary condition, a vacuum layer of 22 \AA was included in the unit cell along the transverse direction to the phosphorene layer. Phosphorus atoms have electron configuration $1s^2 2s^2 2p^6 3s^2 3p^3$, which includes five (valence) electrons at the highest-numbered (third) shell ($3s^2 3p^3$): two and three of them in the $3s$ and $3p$ subshells, respectively. The electron wave functions were expanded in plane waves with a kinetic energy cut-off of 34.414 Ry , while the energy cut-off for the charge density was set to ten times larger. The Brillouin-zone integration was performed by a $10 \times 8 \times 1$ \mathbf{k} -points grid (mesh) following the scheme proposed by Monkhorst–Pack⁸⁶. To simulate the uniaxial or shear strain, we changed or shifted the lattice parameters and defined the strain magnitude ε through its relation with the relative change of the sides (parameters) as expressed in Figs. 2a–d. The structure was allowed to relax (be geometrically optimized) after each step of the strain magnitude for each type and direction of the deformation.

Results and discussion

Before proceeding to study of the strained phosphorene sample, in order to test and validate our numerical model, it is reasonably to consider this material initially at ambient condition, *i.e.*, when it is unstrained. The DFT-based *ab initio* calculations (within QE simulation package) of the energy band structure in Fig. 3a show that the single-layer phosphorene is a semiconductor with a nearly direct band gap at the centre of the Brillouin zone (Γ -point). The calculated band gap is circa 0.945 eV , which agrees with the previous first principals computational results based on the GGA/PBE^{12,28,30,39,47,48,55}. All electronic bands along the S – Y path are double-degenerated. Similar double degeneracy has been also revealed for the phonon dispersion curves (modes)^{10,28}. The high dispersions between Γ and X are observed in Fig. 3a for both valence and conduction bands. For the

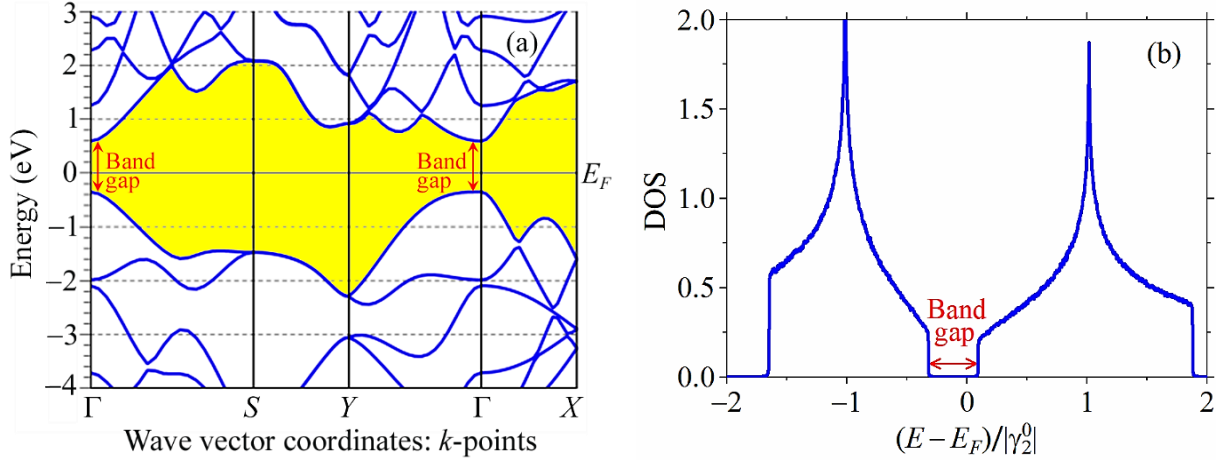


Figure 3. The electron energy, E , band structure (a) and total density of states (b) of unstrained phosphorene calculated within the standard DFT (GGA-PBE) method and TB model, respectively. Shaded (highlighted in yellow online) region is an area between the valence band maximum (located along the highest curve profile below the Fermi level E_F set to be zero) and conduction band minimum (along the lowest curve profile above the E_F).

Γ -to- Y direction, the dispersion is smaller in the conduction band, but strong in the valence band, which is changed from a rather flat near the Γ point to the deep minimum near the Y point.

The band gap value in Fig. 3a contradicts to the gap width, ≈ 1.5 eV, in Fig. 3b, calculated within the framework of TB model, which in turn practically coincides with the experimentally measured gap value² and well agrees with *ab initio* calculations^{10,12,27,28,45} based on the of Heyd–Scuseria–Ernzerhof (HSE)06 hybrid functional⁸⁷. Such an agreement justifies the TB Hamiltonian (1) we used in the model and permits of adequate and accurate results that we expect to obtain for the cases of the strain-affected hopping parameters (2). It is well known from the literature that the standard DFT (based on the PBE pseudopotential) calculations underestimate the band gap in phosphorene. This problem can be solved, *e.g.*, through using the hybrid HSE06 functional^{10,12,27,28,45} or *GW* (instead of GGA) approximation^{48,62,66,67}. Nevertheless, in spite of the gap underestimating, there are no any other significant changes in the electronic structure for the standard global hybrid (PBE) and screened hybrid (HSE06) functionals as well as *GW* correction. Each of them exhibits very similar features and tendencies in the band gap behaviour, including its strain-induced nonmonotonic dependence and direct–indirect gap transition (see, *e.g.*, references in the caption to the figure firstly mentioned in the next paragraph). Therefore, sustaining some other authors^{28,47,48}, we do not focus on this problem, as that is not the scope of this work.

The band gap evolution in phosphorene subjected to uniaxial tensile and shear strains is presented in Fig. 4, where results of our calculations within the TB model (with distant-dependent hopping parameters) and DFT are compared with other computations, where authors used different pseudopotentials, mainly PBE or HSE. In particular, Figs. 4a, b contain comparative results on the uniaxial tensile strains of Wang *et al.* (2015)⁵⁵ and Phuc *et al.* (2018)⁴⁷ who used the PBE pseudopotential method; Peng *et al.* (2014)²⁷, Sa *et al.* (2014)¹⁰, and Li *et al.* (2014)⁴⁵ applied the HSE method; and Hernandez *et al.*⁴⁸ based on the *GW* approach. Figures 4c, d contain comparative results on the shear strains of Ranawat *et al.* (2015)³⁰ and Sa *et al.* (2015)²⁸ based on the PBE pseudopotential, along with results of Sa *et al.* (2015)²⁸ based of HSE method. Note that except Sa *et al.* (2015)²⁸ some other authors^{10,27,48,45,55} also used both types of the pseudopotentials (standard PBE and hybrid HSE) to compare the output computational results on the tensile deformation. However, we do not reproduce them in Figs. 4a, b in order to avoid the figure overload with excessive details and information.

As Figs. 4a–d demonstrate, the tight-binding model results (black solid squares, ■) lead to a linear strain dependence of the electronic band gap for both types and directions of the deformation within the considered strain percentage (up to 15%). The band gap increases or decreases monotonously as the stretching or compression increases or decreases, respectively (Figs. 4a, b).

These findings agree with the linear strain-induced change of the band gap as a result of the combined (valence-force + tight-binding) multi-scale approach of Midtvedt *et al.*⁶³ at small–moderate deformation values (up to 5%) for which the approach is valid. Our TB calculations also sustain numerical results of Midtvedt *et al.*⁶³ on the slightly faster linear change of the band gap for armchair stretching (Fig. 4a) in comparison with the zigzag one (Fig. 4b).

In contrast to the TB-model-based results, the DFT-based calculations predict the nonmonotonic behaviour of the band gap as a function of applied uniaxial tensile deformation along either zigzag direction (Fig. 4a) or armchair one (Fig. 4b) independently on the approximation (GGA or *GW*) and pseudopotential (PBE or HSE06) used. In this respect, our DFT calculations (black solid circles, ●) sustain first principles findings of other authors. We observe the qualitative agreement between our DFT curves and *ab initio* findings based on HSE pseudopotential^{10,27,45} or *GW* approximation⁴⁸ in Figs. 4a, b, and even more or less quantitative coincidence as compared with the PBE-based results^{47,55}. The nonmonotonic behaviour of the strain-dependent band gap as well as its direct–indirect transition is attributed to the changes occurring on different regions of the valence band maximum (VBM) and conduction band minimum (CBM) in the band structure (Fig. 3a). As the uniaxial strain increases, the dispersion on the Γ – X and Γ – Y modes changes, and new maximums and minimums on these paths of the VBM and CBM, respectively, appear, which results to new real (indirect) band gap size smaller than the direct one (in the Γ point)⁴⁸. The complete understanding (explanation) of the reason of the direct–indirect gap transition and its nonmonotone change comes

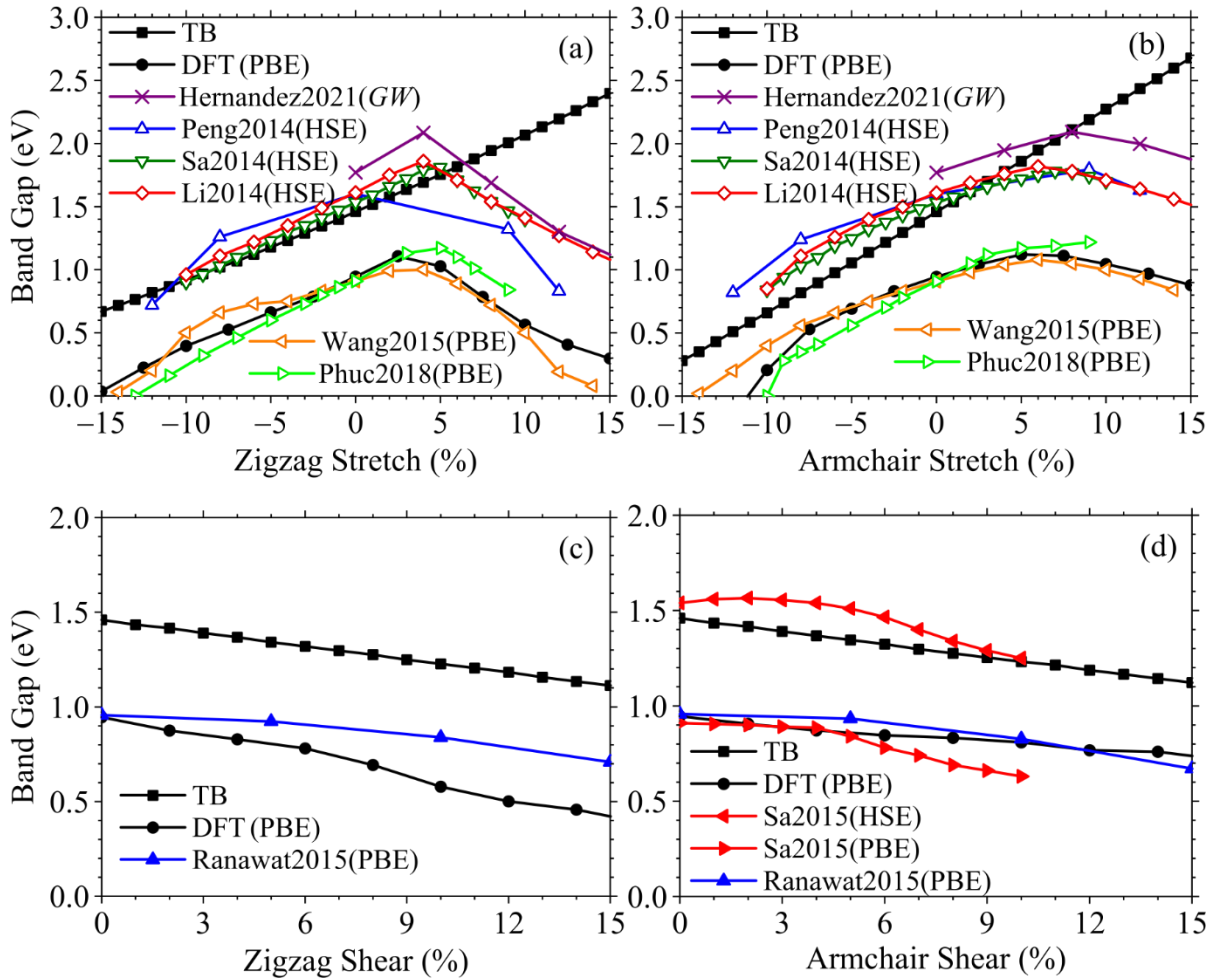


Figure 4. Band gap vs. uniaxial tensile (a, b) and shear (c, d) strains calculated within the tight-binding (TB) model (■) and density functional theory (DFT) method (●) as compared with numerical findings of other authors. Here, Δ —Peng *et al.* (2014)²⁷, ∇ —Sa *et al.* (2014)¹⁰, \diamond —Li *et al.* (2014)⁴⁵, \triangleleft —Wang *et al.* (2015)⁵⁵, \triangleright —Phuc *et al.* (2018)⁴⁷, \times —Hernandez *et al.* (2021)⁴⁸, \blacktriangle —Ranawat *et al.* (2015)³⁰, \blacktriangleleft and \blacktriangleright —Sa *et al.* (2015)²⁸. A colour version of this figure is available online.

from the studying the contributions to the gap size from the s , p_x , p_y , p_z atomic orbitals on the partial (projected) density of states (PDOS)⁴⁸. With an increase of the strain percentage, the orbitals can mix (overlap) to generate the new hybrid orbitals (*i.e.*, undergo the hybridization) near (below or above) the Fermi level with the formation of the new (valence or conduction) band and gap value⁴⁸. Our additional calculations show that the nonmonotonic band gap behaviour can be realizable within the TB model through changing (increasing in several times) the decay rate parameter β in Eq. (2).

Figures 4c, d exhibits evidence of the band gap gradual depletion as the shear deformation increases along either zigzag or armchair direction independently on the model and approximation employed. All three approaches (TB, PBE and HSE) employed for the study yield results, which differ from each other only qualitatively, but not quantitatively. It is expected that the curves reflecting the gap values calculated based on the PBE pseudopotential are lower than those ones obtained based on the HSE functional as well as within the framework of the TB model. As in case of

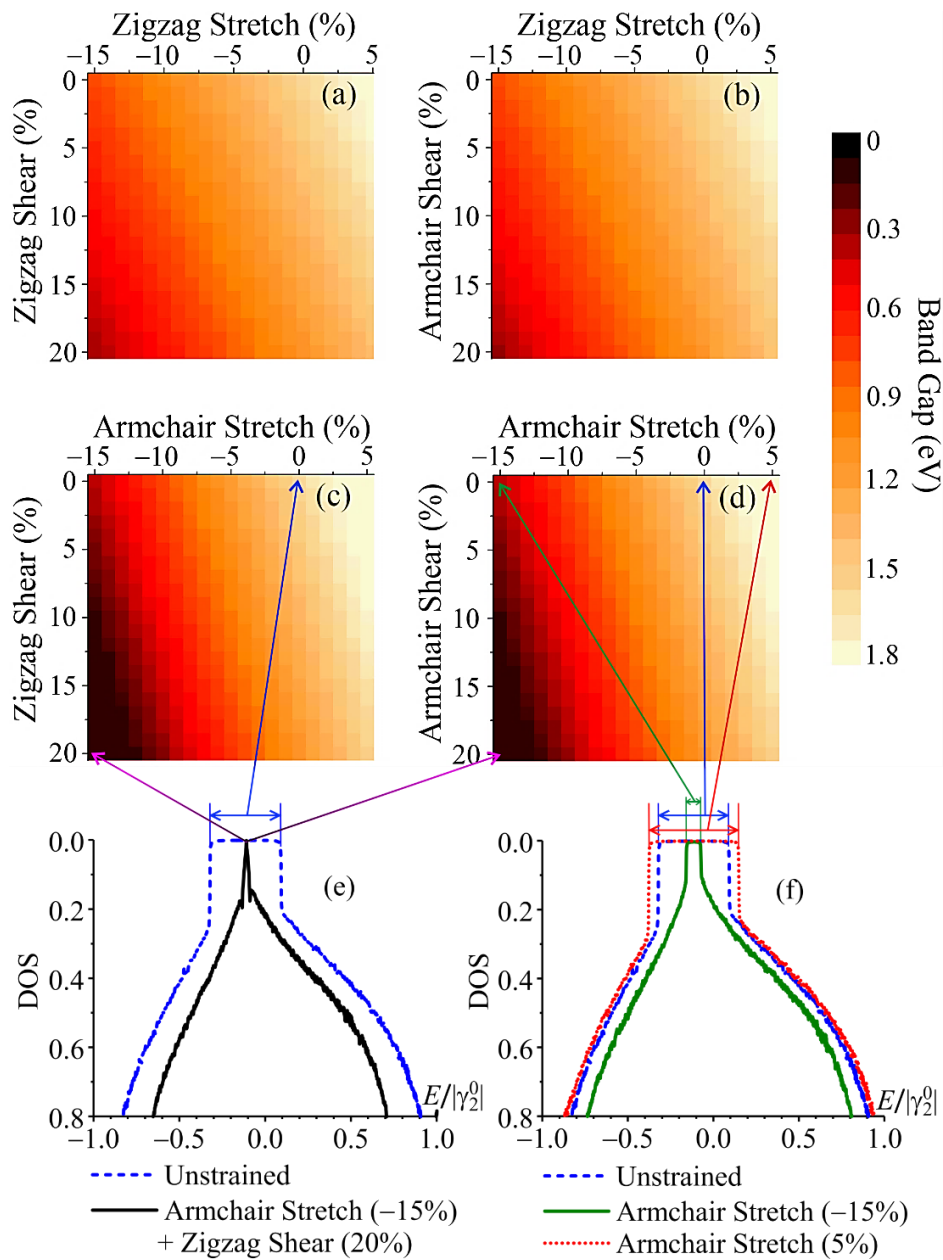


Figure 5. (Colour online) Strain-dependent band-gap patterns for black phosphorene under tensile (compression) and shear deformations (a–d). Representative DOS curves (e, f) demonstrate how the diagrams (a–d) are plotted: each band gap value in (a–d) equals to the plateau (gap) width extracted from the corresponding DOS curve as arrows indicate.

the uniaxial strains, the band gap also experiences the direct-to-indirect transition when the certain percentage of the shear stress is loaded, which is revealed based on the DFT calculations^{28,30} but cannot be detected within the TB model supplemented with the bond-dependent hopping parameters.

The deformation-dependent band-gap patterns in Figs. 5a–d, exhibiting the effect of simultaneous action of both (uniaxial tensile + shear) strain types, are obtained within the TB model. For this purpose, the family of more than four hundreds of densities of states has been calculated for different values and directions of both deformation types. To plot the diagrams, we extracted the band gap size from the calculated DOS curve as depicted in representative Figs. 5e, f. One can observe from Fig. 5 that the band gap closes, — the semiconductor-to-(semi)metal phase transition occurs, — when both strain types are applied: $\approx 15\%$ of the armchair compression + at least $\approx 10\%$ of shearing along any of two (armchair or zigzag) directions. That is the semiconductor–(semi)metal phase transition can be reached at lower percentages of the strains if both deformation types are switched on. Inasmuch as the phosphorene lattice can be unstable under large deformations (*e.g.*, compression)¹⁰, it is important since offers us a possibility to reach the band gap closing within the range of strictly non-destructive deformations of the phosphorene in case of the necessity of the semiconductor-to-(semi)metal phase transition for the practical application.

Conclusions

Monolayer black phosphorene, as a still relatively new member of the $2D$ family, is a remarkably suitable object of the study in the field of $2D$ straintronics on the way of following its main concept: engineering the electronic properties of $2D$ materials by means of the introduction of mechanical deformations. Intraplanar strains, namely, uniaxial tension and shearing, are one of them acting as a powerful tool for tuning the electronic band gap from zero up to the values which are inherent to the wide-band-gap semiconductors (up to 2 eV and above), that is much more higher than for silicon (1.12 eV) commonly used in electronics devices.

To study the effects of the uniaxial tensile strain and shear deformation as well as their combinations on the band gap in phosphorene, the tight-binding Hamiltonian with the distant-dependent hopping integrals is used, and obtained results are compared with both our first-principles calculations and those obtained by other authors. TB model allows to perform calculations with the systems containing millions of atoms (as the real experimental samples contain), and thus is substantially less computationally demanding in comparison with any *ab initio* simulations, restricted to periodic supercells or lattice fragments with a relatively small number of atoms due to the computational expensiveness.

The TB-model-based findings indicate that the band gap value of unstrained phosphorene agrees with both the experimental one and that obtained using the DFT with the screened hybrid (HSE06) functional or *GW* correction, and linearly depends on the both deformation types. Namely, the band gap increases (decreases) as the uniaxial tensile strain increases (decreases), and gradually decreases with increasing the shear deformation. As the decay rate parameter defining the bond-length dependence of the hoppings enhances, the linear dependence of the band gap on the uniaxial tensile strain becomes the non-monotonic one and similar to that obtained from our and other authors' DFT calculations. The nonmonotonic dependence of the band gap with the stretching deformation can be understood from the partial DOS exhibiting the contributions to the gap size from different (s , p_x , p_y , p_z) atomic orbitals that can overlap and hybridize near the Fermi level with the formation of the new band and gap size as the strain percentage grows. Within the TB model, we extract the information on the band gap width from the total DOS, therefore cannot detect the overlapping or hybridization. In case of the shear strain, both (TB and DFT) methods give the gradual degradation of the gap with only difference in its value, which is underestimated for DFT-PBE as compared to the DFT-HSE and TB.

The strain-dependent band-gap pattern diagrams demonstrate the variety of the continuous gap values realizable when a combined (tensile/compression + shear) strain loaded. A semiconductor-to-semimetal phase transition in the phosphorene can be reached at lower percentages of the strains if both deformation types (stretching + shearing) are switched on. It offers us a possibility to reach the bandgap closing at lower (strictly non-destructive) deformations of the phosphorene, if such a transition appears to be useful for overcoming of the challenges dealing with modification of its properties and functionalization.

Competing interests

The authors declare no competing interests.

Acknowledgements

The first author acknowledges the National Academy of Sciences of Ukraine for support within the framework of the program of post-doctoral research in the N.A.S. of Ukraine for 2021–2023 through the project “Complex diagnostics of sensitive to strains and defects structural and electronic properties of metallic nanomaterials” (state reg. No. 0120U102265). The third and fourth authors acknowledge the National Academy of Sciences of Ukraine for support within the departmental research for 2022–2026 (state reg. No. 0122U002396). All authors obliged to the Armed Forces of Ukraine for providing security made possible to perform this work.

Author contributions

A.G.S. and I.Y.S. performed numerical calculations using the DFT-based QE simulation package and TB-model-based computations, respectively. T.M.R. designed the project, reviewed the literature, collected data, supervised the findings of this work, and wrote the manuscript with input from all authors. V.A.T. supervised the project, devised the main conceptual ideas, verified analytical approaches, and provided critical feedback. All authors were in charge of the overall direction and planning, analysed and discussed the results, commented on the manuscript, and contributed to its final version.

Data availability

The data that support the findings of this study available from the corresponding author on reasonable request.

References

1. In the literature, the term “2D materials” refers to those systems thermodynamically stable in one or just a few atomic layers (planes) thick (*e.g.*, graphene — one atomic plane; phosphorene — two atomic plane) and possessing properties that differ from their bulk layered analogues (graphite, phosphorus).
2. Liu, H. *et al.* Phosphorene: an unexplored 2D semiconductor with a high hole mobility. *ACS Nano* **8**, 4033–4041, <https://doi.org/10.1021/nn501226z> (2014).
3. Li, L. *et al.* Black phosphorus field-effect transistors. *Nature Nanotech.* **9**, 372–377, <https://doi.org/10.1038/nnano.2014.35> (2014).
4. Bridgman, P. W. Two new modifications of phosphorus. *J. Am. Chem. Soc.* **36** (7), 1344–1363, <https://doi.org/10.1021/ja02184a002> (1914).
5. Bridgman, P. W. Further note on black phosphorus. *J. Am. Chem. Soc.* **38** (3), 609–612, <https://doi.org/10.1021/ja02260a008> (1916).
6. Liu, H., Du, Y. C., Deng, Y. X. & Ye, P. D., Semiconducting black phosphorus: synthesis, transport properties and electronic applications. *Chem. Soc. Rev.* **44** (9), 2732, <https://doi.org/10.1039/C4CS00257A> (2015).
7. Zhu, X. J. *et al.* Black phosphorus revisited: a missing metal-free elemental photocatalyst for visible light hydrogen evolution. *Adv. Mater.* **29** (17), 1605776 (2017). <https://doi.org/10.1002/adma.201605776>
8. Piro, N. A., Figueroa, J. S., McKellar, J. T. & Cummins, C. C. *Science* **313** (5719), 1276, <https://doi.org/10.1126/science.1129630> (2006).
9. Wu, S., Hui, K. S. & Hui, K. N. 2D black phosphorus: from preparation to applications for electrochemical energy storage. *Adv. Sci.* **5**, 1700491, <https://doi.org/10.1002/advs.201700491> (2018).
10. Sa, B., Li, Y.-L., Qi, J., Ahuja, R. & Sun Z. Strain engineering for phosphorene: the potential application as a photocatalyst. *J. Phys. Chem. C* **118** (46) 26560–26568, <https://doi.org/10.1021/jp508618t> (2014).
11. Jing, Y., Zhang, X. & Zhou, Z. Phosphorene: what can we know from computations? *Wiley Interdisciplinary Reviews: Comput. Mol. Sci.* **6** (1), 5–19, <https://doi.org/10.1002/wcms.1234> (2016).
12. Çakır, D., Sahin, H. & Peeters, F. M. Tuning of the electronic and optical properties of single-layer black phosphorus by strain. *Phys. Rev. B* **90** (20), 205421, <https://doi.org/10.1103/PhysRevB.90.205421> (2014).

13. Liang, L. *et al.* Electronic bandgap and edge reconstruction in phosphorene materials. *Nano Lett.* **14** (11), 6400–6406, <https://doi.org/10.1021/nl502892t> (2014).
14. Wang, X. *et al.* Highly anisotropic and robust excitons in monolayer black phosphorus. *Nature Nanotech* **10**, 517–521, <https://doi.org/10.1038/nnano.2015.71> (2015).
15. Keyes, R. W. The electrical properties of black phosphorus. *Phys. Rev.* **92** (3), 580–584, <https://doi.org/10.1103/PhysRev.92.580> (1953).
16. Warschauer, D. Electrical and optical properties of crystalline black phosphorus. *J. Appl. Phys.* **34** (7), 1853–1860, <https://doi.org/10.1063/1.1729699> (1963).
17. Narita, S. *et al.* Electrical and optical properties of black phosphorus single crystals. *Physica B+C* **117–118**, Pt. 1, 422–424, [https://doi.org/10.1016/0378-4363\(83\)90547-8](https://doi.org/10.1016/0378-4363(83)90547-8) (1983).
18. Maruyama, Y., Suzuki, S., Kobayashi, K. & Tanuma, S. Synthesis and some properties of black phosphorus single crystals. *Physica B+C* **105**, 99–102, [https://doi.org/10.1016/0378-4363\(81\)90223-0](https://doi.org/10.1016/0378-4363(81)90223-0) (1981).
19. Carvalho, A. *et al.* Phosphorene: from theory to applications. *Nature Rev. Mater.* **1**, 16061, <https://doi.org/10.1038/natrevmats.2016.61> (2016).
20. Chaudhary, V., Neugebauer, P., Mounkachi, O., Lahbabi, S. & Fatimy, A. El. Phosphorene — an emerging two-dimensional material: recent advances in synthesis, functionalization, and applications. *2D Mater.* **9** (3), 032001, <https://doi.org/10.1088/2053-1583/ac6dc2> (2022).
21. Akhtar, M. *et al.* Recent advances in synthesis, properties, and applications of phosphorene. *npj 2D Mater. Appl.* **1**, 1–13, <https://doi.org/10.1038/s41699-017-0007-5> (2017).
22. Cao, X. & Guo, J. Simulation of phosphorene field-effect transistor at the scaling limit. *IEEE Trans. Electron Devices* **62**, 659–65, <https://doi.org/10.1109/TED.2014.2377632> (2015).
23. Chowdhury, C. & Datta, A. Exotic physics and chemistry of two-dimensional phosphorus: phosphorene. *J. Phys. Chem. Lett.* **8** (13), 2909, <https://doi.org/10.1021/acs.jpcclett.7b01290> (2017).
24. Jiang, J.-W. & Park, H. S. Mechanical properties of single-layer black phosphorus. *J. Phys. D: Appl. Phys.* **47** (38), 385304, <https://doi.org/10.1088/0022-3727/47/38/385304> (2014).
25. Kou, L., Chen, C. & Smith, S. C. Phosphorene: fabrication, properties, and applications. *J. Phys. Chem. Lett.*, **6** (14), 2794–2805, <https://doi.org/10.1021/acs.jpcclett.5b01094> (2015).
26. Wei, Q. & Peng, X. Superior mechanical flexibility of phosphorene and few-layer black phosphorus. *Appl. Phys. Lett.* **104** (25), 251915, <https://doi.org/10.1063/1.4885215> (2014).
27. Peng, X., Wei, Q. & Copple, A. Strain-engineered direct-indirect band gap transition and its mechanism in two-dimensional phosphorene. *Phys. Rev. B* **90** (8), 085402, <https://doi.org/10.1103/PhysRevB.90.085402> (2014).
28. Sa, B., Li, Y.-L., Sun, Z., Qi, J., Wen, C. & Wu, B. The electronic origin of shear-induced direct to indirect gap transition and anisotropy diminution in phosphorene. *Nanotechnology* **26** (21), 215205, <https://doi.org/10.1088/0957-4484/26/21/215205> (2015).
29. Hatam-Lee, S. M., Peer-Mohammadi, H. & Rajabpour, A. Tuning shear mechanical properties and tensile strength anisotropy of monolayer black phosphorene: a molecular dynamics study. *Mater. Today Commun.* **26**, 101796, <https://doi.org/10.1016/j.mtcomm.2020.101796> (2021).
30. Ranawat, Y. S., Jain, R. Effect of shear strain on band structure and electronic properties of phosphorene. Preprint at <https://doi.org/10.48550/arXiv.1512.05392> (2015).
31. Hu, T., Han Y. & Dong, J. Mechanical and electronic properties of monolayer and bilayer phosphorene under uniaxial and isotropic strains. *Nanotechnology* **25** (45), 455703, <https://doi.org/10.1088/0957-4484/25/45/455703> (2014).
32. Szroeder, P. *et al.* Effect of uniaxial stress on the electrochemical properties of graphene with point defects, *Appl. Surf. Sci.* **442**, 185–188, <https://doi.org/10.1016/j.apsusc.2018.02.150> (2018).
33. Radchenko, T.M. *et al.* Defect-pattern-induced fingerprints in the electron density of states of strained graphene layers: diffraction and simulation methods, *Phys. Status Solidi B* **256** (5), 1800406, <https://doi.org/10.1002/pssb.201800406> (2019).
34. Sagalianov, I.Yu., Radchenko, T.M., Prylutsky, Yu.I., Tatarenko, V.A. & Szroeder, P. Mutual influence of uniaxial tensile strain and point defect pattern on electronic states in graphene. *Eur. Phys. J. B* **90** (6), 112, <https://doi.org/10.1140/epjb/e2017-80091-x> (2017).
35. Sahalianov, I.Yu., Radchenko, T.M., Tatarenko, V.A., Cuniberti, G. & Prylutsky, Yu.I. Straintronics in graphene: extra large electronic band gap induced by tensile and shear strains, *J. Appl. Phys.* **126** (5), 054302, <https://doi.org/10.1063/1.5095600> (2019).
36. Miao, F., Liang, S.J. & Cheng, B. Straintronics with van der Waals materials. *npj Quantum Mater.* **6**, 59, <https://doi.org/10.1038/s41535-021-00360-3> (2021).
37. Lin, Z. *et al.* Research update: recent progress on 2D materials beyond graphene: From ripples, defects, intercalation, and valley dynamics to straintronics and power dissipation featured. *APL Mater.* **6**, 080701,

-
- <https://doi.org/10.1063/1.5042598> (2018).
38. Jiang, J. W. & Park, H. Negative poisson's ratio in single-layer black phosphorus. *Nature Commun.* **5**, 4727, <https://doi.org/10.1038/ncomms5727> (2014).
 39. Elahi, M., Khaliji, K., Tabatabaei, S. M., Pourfath M. & Asgari, R. Modulation of electronic and mechanical properties of phosphorene through strain. *Phys. Rev. B* **91** (11), 115412, <https://doi.org/10.1103/PhysRevB.91.115412> (2015).
 40. Du, Y. et al. Auxetic black phosphorus: a 2D material with negative Poisson's ratio. *Nano Lett.*, **16** (10), 6701–6708, <https://doi.org/10.1021/acs.nanolett.6b03607> (2016).
 41. Sahalianov, I.Yu., Radchenko, T.M., Tatarenko, V.A. & Prylutsky, Yu.I. Magnetic field-, strain-, and disorder-induced responses in an energy spectrum of graphene. *Annals of Physics* **398**, 80–93, <https://doi.org/10.1016/j.aop.2018.09.004> (2018).
 42. Szroeder, P., Sahalianov, I., Radchenko, T., Tatarenko, V. & Prylutsky, Yu. The strain- and impurity-dependent electron states and catalytic activity of graphene in a static magnetic field, *Optical Materials*, **96**, 109284, <https://doi.org/10.1016/j.optmat.2019.109284> (2019).
 43. Rodin, A. S., Carvalho, A. & Castro Neto, A. H. Strain-induced gap modification in black phosphorus. *Phys. Rev. Lett.* **112**, 176801, <https://doi.org/10.1103/PhysRevLett.112.176801> (2014).
 44. Hien, N. D., Davoudiniya, M., Mirabbaszadeh, K., Phuong, Le T.T. & Yarmohammadi, M. Strain-induced electronic phase transition in phosphorene: a Green's function study. *Chemical Phys.* **522**, 249–255, <https://doi.org/10.1016/j.chemphys.2019.03.013> (2019).
 45. Li, Y., Yang, S. & Li, J. Modulation of the electronic properties of ultrathin black phosphorus by strain and electrical field. *J. Phys. Chem. C* **118** (41), 23970–23976, <https://doi.org/10.1021/jp506881v> (2014).
 46. Yarmohammadi, M., Mortezaei, M. & Mirabbaszadeh, K. Anisotropic basic electronic properties of strained black phosphorene, *Physica E* **124**, 114323, <https://doi.org/10.1016/j.physe.2020.114323> (2020).
 47. Phuc, H. V., Hieu, N. N., Ilyasov, V. V., Le Phuong, T. T., Nguyen, C. V. First principles study of the electronic properties and band gap modulation of two-dimensional phosphorene monolayer: effect of strain engineering. *Superlattices and Microstructures* **118**, 289–297, <https://doi.org/10.1016/j.spmi.2018.04.018> (2018).
 48. Hernandez, J. M., Guerrero-Sanchez, J., Fernandez-Escamilla, H. N., Hernandez-Cocolezzi, G. & Takeuchi, N. First-principles studies of the strain-induced band-gap tuning in black phosphorene, *J. Phys.: Condens. Matter* **33** (17), 175502, <https://doi.org/10.1088/1361-648X/abdd62> (2021).
 49. Fei, R. & Yang, L. Strain-engineering the anisotropic electrical conductance of few-layer black phosphorus. *Nano Lett.* **14** (5), 2884–2889, <https://doi.org/10.1021/nl500935z> (2014).
 50. Radchenko, T.M., Tatarenko, V.A. & Cuniberti, G. Effects of external mechanical or magnetic fields and defects on electronic and transport properties of graphene, *Mater. Today: Proc.* **35**, 523–529, <https://doi.org/10.1016/j.matpr.2019.10.014> (2021).
 51. Sahalianov, I.Yu., Radchenko, T.M., Tatarenko, V.A. & Cuniberti, G. Sensitivity to strains and defects for manipulating the conductivity of graphene, *EPL* **132** (4), 48002, <https://doi.org/10.1209/0295-5075/132/48002> (2020).
 52. Solomenko, A.G., Balabai, R.M., Radchenko, T.M. & Tatarenko, V.A. Functionalization of quasi-two-dimensional materials: chemical and strain-induced modifications. *Prog. Phys. Met.* **23** (2), 147–238, <https://doi.org/10.15407/ufm.23.02.147> (2022).
 53. Jiang, J.-W. & Park, H. S. Analytic study of strain engineering of the electronic bandgap in single-layer black phosphorus. *Phys. Rev. B* **91**, 235118, <https://doi.org/10.1103/PhysRevB.91.235118> (2015).
 54. Wang, L., Kutana, A. Zou, X. & Yakobson, B. I. Electro-mechanical anisotropy of phosphorene. *Nanoscale* **7** (21), 9746–9751, <https://doi.org/10.1039/C5NR00355E> (2015).
 55. Wang, C., Xia, Q., Nie, Y. & Guo, G. Strain-induced gap transition and anisotropic Dirac-like cones in monolayer and bilayer phosphorene. *J. Appl. Phys.* **117** (12), 124302, <https://doi.org/10.1063/1.4916254> (2015).
 56. Baghsiyahi, F. B. & Yeganeh, M. The effect of strain on the zigzag and armchair phosphorene nanoribbon. *Physica E* **121**, 114088, <https://doi.org/10.1016/j.physe.2020.114088> (2020).
 57. Zhang, Z., Zhao, Y. & Ouyang, G. Strain modulation of electronic properties of monolayer black phosphorus. *J. Phys. Chem. C* **121** (35), 19296–19304, <https://doi.org/10.1021/acs.jpcc.7b06342> (2017).
 58. Balabai, R. M. & Solomenko, A. G. Use of the adsorbed organic molecules as dopants for creation of the built-in lateral *p-n* junctions in a sheet of black phosphorene. *J. Nano- Electron. Phys.* **11** (5), 05033, [https://doi.org/10.21272/jnep.11\(5\).05033](https://doi.org/10.21272/jnep.11(5).05033) (2019).
 59. Balabai, R., Solomenko, A. & Kravtsova, D. Electronic and photonic properties of lateral heterostructures based on functionalized graphene depending on the degree of fluorination. *Mol. Cryst. Liq. Cryst.* **673** (1), 125–136, <https://doi.org/10.1080/15421406.2019.1578502> (2018).

-
60. Balabai, R. M. & Lubenets, A. G. Lateral junctions based on graphene with different doping regions. *J. Nano- Electron. Phys.* **9** (5), 05017, [https://doi.org/10.21272/jnep.9\(5\).05017](https://doi.org/10.21272/jnep.9(5).05017) (2017)
 61. Li, S., Liu, X., Li, R. & Su, Y. Shear deformation dominates in the soft adhesive layers of the laminated structure of flexible electronics. *Int. J. Solids Struct.* **110–111**, 305–314, <https://doi.org/10.1016/j.ijsolstr.2016.12.006> (2017).
 62. Rudenko, A. N. Yuan, S. & Katsnelson, M. I. Toward a realistic description of multilayer black phosphorus: from GW approximation to large-scale tight-binding simulations. *Phys. Rev. B* **92** (8) 085419, <https://doi.org/10.1103/PhysRevB.92.085419> (2015); Erratum *Phys. Rev. B* **93** (19), 199906, <https://doi.org/10.1103/PhysRevB.93.199906> (2016)
 63. Midtvedt, D., Lewenkopf, C. H. & Croy, A. Multi-scale approach for strain-engineering of phosphorene. *J. Phys.: Condens. Matter* **29** (18), 185702, <https://doi.org/10.1088/1361-648X/aa66d4> (2017).
 64. Yuan, Y. & Cheng, F. Strain modification on electronic transport of the phosphorene nanoribbon. *AIP Advances* **7** (7), 075310, <https://doi.org/10.1063/1.4991494> (2017).
 65. Madas, S., Mishra, S.K., Kahaly, S. & Upadhyay Kahaly, M. Superior photo-thermionic electron emission from illuminated phosphorene surface. *Sci. Rep.* **9**, 103107, <https://doi.org/10.1038/s41598-019-44823-x> (2019).
 66. Rudenko, A. N. & Katsnelson, M. I. Quasiparticle band structure and tight-binding model for single- and bilayer black phosphorus. *Phys. Rev. B* **89** (20), 201408(R), <https://doi.org/10.1103/PhysRevB.89.201408> (2014).
 67. Yuan, S., Rudenko, A. N. & Katsnelson, M. I. Transport and optical properties of single- and bilayer black phosphorus with defects. *Phys. Rev. B* **91** (11), 115436, <https://doi.org/10.1103/PhysRevB.91.115436> (2015).
 68. Taghizadeh Sisakht, E., Fazileh, F., Zare, M. H., Zarenia, M. & Peeters, F. M. Strain-induced topological phase transition in phosphorene and in phosphorene nanoribbons. *Phys. Rev. B* **94** (8), 085417, <https://doi.org/10.1103/PhysRevB.94.085417> (2016).
 69. Midtvedt, D. & Croy, A. Valence-force model and nanomechanics of single-layer phosphorene. *Phys. Chem. Chem. Phys.* **18** (33), 23312–23319 <https://doi.org/10.1039/C6CP04361E> (2016).
 70. Midtvedt, D., Lewenkopf, C. H. & Croy, A. Strain–displacement relations for strain engineering in single-layer 2D materials. *2D Mater.* **3** (1), 011005, <https://doi.org/10.1088/2053-1583/3/1/011005> (2016).
 71. The decay rate magnitude β is discussable since there is no an experiment from which this value can be extracted as it has been done for graphene. For the phosphorene, due to its puckered structure, this value is assumed to be lower in comparison with that (≈ 3.37) appropriated for a flat graphene structure^{34,35}.
 72. Mohammadi, Y. & Nia, B. A. Strain engineering the charged-impurity-limited carrier mobility in phosphorene. *Superlattices and Microstructures* **89**, 204, <https://doi.org/10.1016/j.spmi.2015.10.049> (2016).
 73. Harrison, W. A. *Elementary Electronic Structure* (World Scientific, Singapore, 1999).
 74. Radchenko, T. M., Shylau, A. A. & Zozoulenko, I. V. Conductivity of epitaxial and CVD graphene with correlated line defects, *Solid State Commun.* **195**, 88–94, <https://doi.org/10.1016/j.ssc.2014.07.012> (2014).
 75. Sutton, A. P. *Electronic Structure of Materials* (Oxford University Press, Oxford, 1993).
 76. Mahan, G. D. *Many Particle Physics* (Plenum Press: New York, 1993).
 77. Giannozzi, P. *et al.* QUANTUM ESPRESSO: a modular and open-source software project for quantum simulations of materials. *J. Phys.: Condens. Matter* **21** (39), 395502, <https://doi.org/10.1088/0953-8984/21/39/395502> (2009).
 78. Kohn, W. & Sham, L. J. Self-consistent equations including exchange and correlation effects. *Phys. Rev.* **140** (4A), A1133–A1138, <https://doi.org/10.1103/PhysRev.140.A1133> (1965).
 79. Blöchl, P. E. Projector augmented-wave method. *Phys. Rev. B* **50** (24), 17953, <https://doi.org/10.1103/PhysRevB.50.17953> (1994).
 80. Perdew, J. P., Burke, K. & Ernzerhof, M. Generalized gradient approximation made simple. *Phys. Rev. Lett.* **77** (18), 3865–3868, <https://doi.org/10.1103/PhysRevLett.77.3865> (1996).
 81. Perdew, J. P. *et al.* *Phys. Rev. B* **46** (11), 6671–6687, <https://doi.org/10.1103/PhysRevB.46.6671> (1992).
 82. Perdew, J. P. & Wang, Y. Accurate and simple analytic representation of the electron-gas correlation energy. *Phys. Rev. B* **45** (23), 13244, <https://doi.org/10.1103/PhysRevB.45.13244> (1992).
 83. Ernzerhof, M. & Scuseria, G. E. Assessment of the Perdew–Burke–Ernzerhof exchange–correlation functional. *J. Chem. Phys.* **110** (11), 5029–5036, <https://doi.org/10.1063/1.478401> (1999).
 84. Perdew, J. P., Burke, K., & Wang, Y. Generalized gradient approximation for the exchange–correlation hole of a many-electron system. *Phys. Rev. B* **54** (23), 16533, <https://doi.org/10.1103/PhysRevB.54.16533> (1996).
 85. Cartz, L., Srinivasa, S.R., Riedner, R.J., Jorgensen, J.D. & Worlton, T.G. Effect of pressure on bonding

-
- in black phosphorus. *J. Chem. Phys.* **71** (4), 1718–1721, <https://doi.org/10.1063/1.438523> (1979).
86. Monkhorst, H. J. & Pack, J. D. Special points for Brillouin-zone integrations. *Phys. Rev. B* **13** (12), 5188–5192, <https://doi.org/10.1103/PhysRevB.13.5188> (1976).
87. Paier, J. *et al.* Screened hybrid density functionals applied to solids. *J. Chem. Phys.* **124** (15), 154709, <https://doi.org/10.1063/1.2187006> (2006)